A particle-free stereo-video free-surface reconstruction method for wave-tank experiments

Le Page Sacha [1, *], Tassin Alan [1, *], Caverne Julien [1], Ducrozet Guillaume [2]

[1] Ifremer, RDT Research and Technological Development, F-29280, Plouzané, France
[2] Nantes Université, École Centrale Nantes, CNRS, LHEEA, UMR 6598, F-44000, Nantes, France

* Corresponding authors : Sacha Le Page, email address : lepage.sacha@yahoo.fr ; Alan Tassin, email address : atassin@ifremer.fr

Abstract :

This paper introduces a new stereo-video-based free-surface reconstruction system developed for wave-tank experiments. The originality of the proposed approach relies on the use of short water waves and an adapted lighting system to create a fine texture suitable for the cross-correlation of the stereo image pairs. The feasibility of the approach is demonstrated experimentally in a wave flume. The accuracy of the stereo-video free-surface reconstruction method is assessed through comparisons with measurements performed with a servo-controlled wave gauge. The reconstruction of the free surface at rest and during different regular (periodic) long-crested wave experiments are considered for this purpose. The results demonstrate that, with a suitable free-surface roughness, the accuracy of the stereo-system can be similar to the accuracy of the wave gauge. The accuracy, the simplicity and the flexibility of the approach, which does not necessitate any seeding or dying of the water, nor the use of a laser light source, make it a promising measurement technique for water-wave experiments.

1 Introduction

Experimental investigations on non-linear water-wave propagation [1], complex short crested wave fields [2] and diffracted-radiated wave fields around marine structures [3] necessitate high-resolution spatial and temporal discretization measurement techniques. For decades, the only instruments available for the measurement of water waves were wave gauges measuring locally the water elevation. Until recently, the only way of characterising finely the shape of a free surface was to use a high number of wave gauges. For example, Swan and Sheikh [3] performed experiments with an array of wave probes in order to reconstruct the free-surface elevation around a vertical cylinder interacting with water waves. By repeating the experiments with the same wave conditions, but with a different wave-probe array location, they managed to record the free-surface elevation at over 1400 locations around the cylinder. More than 250 experiment repeats for each wave condition are reported by the authors for this tedious work.

As an alternative to standard local wave gauge measurements, optical image based approaches offer new possibilities and have been strongly developed in the last two to three decades. An extensive review of "Free-surface flow measurements by non-intrusive methods" has been performed recently by Gomit *et. al* . [4]. Among these techniques, one may distinguish different families depending on the principles of the technique. Schlieren techniques (*e.g.* [5]) and stereo-refraction techniques (*e.g.* [6]) make use of the refraction of light through the interface to infer the shape of the free-surface. Stereo-reconstruction and stereo-Particle Image Velocimetry (PIV) approaches require the generation of a diffuse pattern at the free-surface. Different approaches such as the seeding of floating particles [7], the generation of thermal markers using an infra-red laser [8] or the projection of a visible light pattern on the surface of an opaque liquid [9] have been used for this purpose.

Reflection and refraction based methods are very sensitive to small interface perturbations and are therefore a very powerful tool for moderately steep water waves. However, this kind of approaches may become problematic for very steep waves. For refraction techniques based on aerial video cameras and an underwater pattern, the angle of total reflection between water and air may be reached, or the refracted light rays may be so much deviated so that they do not reach the camera. Similarly, for reflection based techniques where the video camera and the light source are in air, the light rays of the source may be so much deviated that they do not reach the video camera.

Different problems are reported in the literature with particle based approaches. The drifting of the particles can lead to a segregation of the particles [10, 11] with strongly inhomogeneous particle densities, the particles may agglomerate [4, 10, 12] or sink below the free-surface in some cases [11]. From a practical point of view, the use of particles may become very tidious if one has to remove them from the tank after the experiments. The projection of a diffuse pattern on the free-surface requires the addition of dye in the water, which can be prohibitive because of the size of the wave tank or because it is simply not compatible with other usages of the tank. The thermal marking approach involves the use of two infra-red video cameras and

a powerful invisible laser source, which makes it rather expensive and dangerous in terms of usage.

In this article, we present a new stereo-video approach for wave tank experiments which aims at circumventing the disadvantages of the different approaches. The idea is to recreate the favorable conditions for the stereo-video reconstruction of the free-surface which are encountered *in situ*. Indeed, [13] and [14] have shown that it was possible to reconstruct the free-surface of water waves at sea with a rather standard stereo-video set-up. The main difference between water waves at sea and in a wave tank is the roughness of the free-surface. At sea, the gravity surface waves interact with the wind which creates shorter waves on top of the surface gravity waves, whereas the free-surface of the water waves generated in standard laboratory conditions (without wind) are very smooth . The smoothness of the air-water interface leads to the specular reflection of the light rays that come from the air and to the refraction of the light rays that come from the water. As a result, in ambient light conditions, a camera placed above the water surface and oriented towards the free surface will see both the reflections of the surrounding objects (in air) on the free-surface and the bottom of the water tank. This difficulty has been reported by several authors (*e.g.* [15]) who tried to validate their stereo-video wave acquisition system in a wave tank before performing measurements at sea. The proposed approach relies on the generation of short water waves with a wave length about one or two orders of magnitude shorter than the wave length of the surface gravity waves of interest and the use of a white diffusive screen placed in front of the cameras. The feasibility of the approach is demonstrated via the reconstruction of a still water plane and of different regular (periodic) waves in a medium scale wave flume. The accuracy of the stereo-video measurements is assessed through comparisons between wave gauge measurements performed in different regions of the reconstruction.

The paper is organized as follows. The stereo-video measurement technique is described in section 2. The accuracy of the stereo-video measurements is analyzed in section 3. Eventually, conclusions and prospects are drawn in section 4.

2 Description of the measurement technique

2.1 Principles of the measurement technique

The principles of the measurement technique is based on a reproduction in laboratory conditions of what we assume to be happening in the *in situ* investigations of [13, 14]. Let us consider that the water waves that we are interested in are perturbed by short waves whose wavelength is one or two orders of magnitude shorter than the waves of interest, as depicted in figure 1 which represents a side view representation of the experimental set-up. By placing a video camera on one side of the tank and creating a diffuse artificial sky on the other side of the tank, one can expect to recreate the conditions of measurements at sea. With this set-up, it is assumed that the difference of intensity of the reflection of the artificial sky on the crests and the troughs of the short waves will lead to a contrasted image on the video camera. If a second camera is placed close to the first camera with a small angle with respect to the direction of the first camera, one can expect that the bright and dark areas on both cameras will
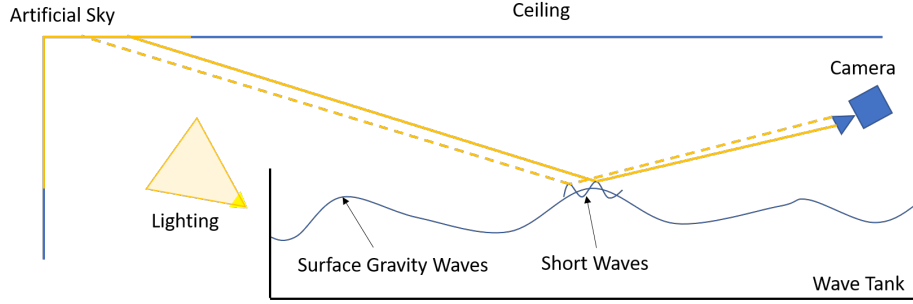
Fig. 1: Principles of texture and lighting conditions for stereo-video free-surface measurements in test tank facilities

originate from the same crests and troughs, hence reproducing the conditions of an apparent diffuse reflection at the free-surface. Note that the luminance of the artificial sky must be sufficiently homogeneous and the amplitude of the short waves must be sufficient to ensure these conditions.

2.2 Experimental implementation of the method in a wave flume

In order to demonstrate the feasibility of the method illustrated in figure 1, we have conducted an experimental campaign in the wave flume of Ifremer in Plouzané, France. The waves are generated by a piston-type wave generator composed of 8 segments over the tank width. The wave generator is installed at one end of the flume and a damping beach is located 40.5 m away, at the other end of the flume. The flume is 4 m wide and the water depth is approximately equal to 2 m in the experiment. Note that different preliminary tests have been performed beforehand (see [16]).

A picture of the experimental set-up is presented in figure 2 and side and top view diagrams are depicted in in figure 3. The experimental set-up is composed of two high-speed video cameras (PHOTRON FASTCAM MINI AX200) equipped with 35 mm lenses installed 23 m from the wave generator, 1.7 m above the free-surface, in the median axis of the flume, facing the wave propagation direction. The grazing angle, *i.e.* the relative angle between the optical axis and the still free-surface, is about 34°. The baseline, *i.e.*, the distance between optic center of each camera, is 393.7 mm. Following [14], the baseline was set to approximately 10% of the distance between the camera and the observed area (the furthest measured point is about 4 m away from the cameras in our case). Both cameras are synchronized and triggered simultaneously with the same analog signal.

The stereo camera calibration is done with a 405 mm × 360 mm checkerboard using MATLAB© Stereo Camera Calibrator [17], based on the approaches of Bouguet [18], Zhang [19], and Heikkila et al [20]. The results show that both cameras have low distortion and the reprojection error is very low (0.04 px).

With the aim of comparing measurements done with our stereo-video free-surface reconstruction system, a servo-controlled wave gauge is set above the measured area
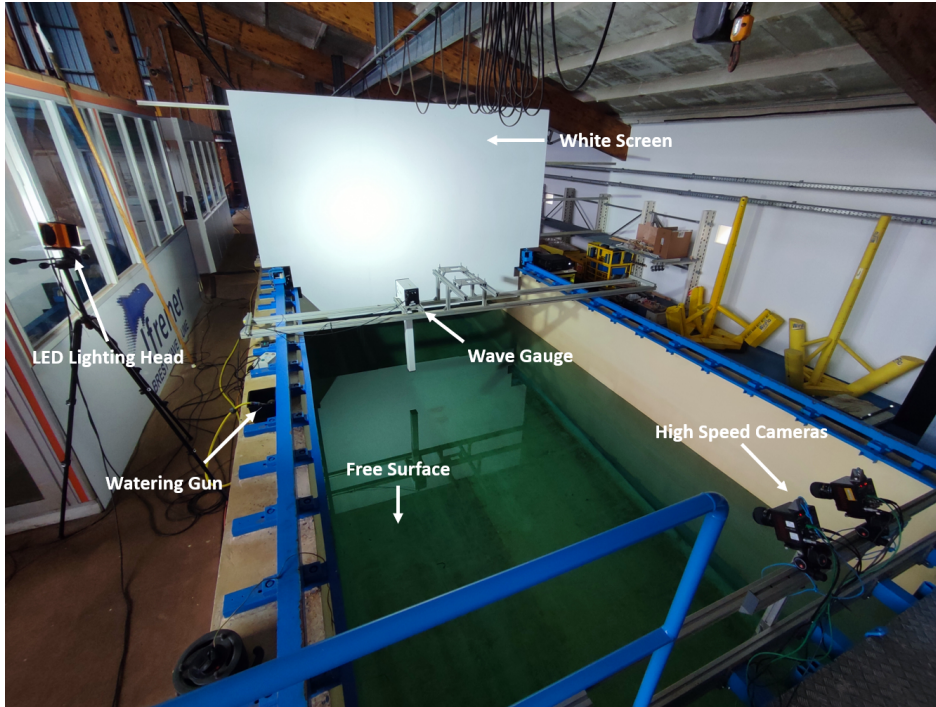
**Fig. 2**: Experimental setup in Ifremer's wave flume, Plouzané, France

(see figure 2). The measurements are performed with a GEN7 HBM recorder. The sampling frequency chosen for the wave gauge and the frame rate of the camera were set to 125 Hz. The wave gauge acquisition is triggered by the wave generator start. The trigger signal, which starts the recording of the video cameras, is also recorded in order to synchronize and compare the different measurements.

As explained in section 2.1, an artificial sky is necessary to produce a diffuse uniform and distant lighting over the measured free surface. For this experimental campaign, a 3 m by 4.6 m matt white screen installed about 5 m from the cameras constitutes our artificial sky. It is illuminated by a LED lighting head, either placed behind the cameras or on the side of the flume.

The texture on the free surface is obtained by watering the free surface with a light rain whose droplet impacts generate short waves on the free surface. The light rain is produced using a watering gun. To cover a larger surface in a uniform way, a sweeping motion is manually given to the watering gun. The size of the droplets is an important parameter. It needs to be sufficiently small so that the short waves generated by the impacts on the free surface do not disturb the waves of interest, *i.e.*, the gravity wave generated by the wave generator. The effect of the light rain droplet impacts on the free surface is illustrated in figure 4 which compares camera views of the free surface, without and with short waves. One can see that the specular reflections of the wave gauge on the free surface and the bottom of the flume, both visible in figure 4a, are
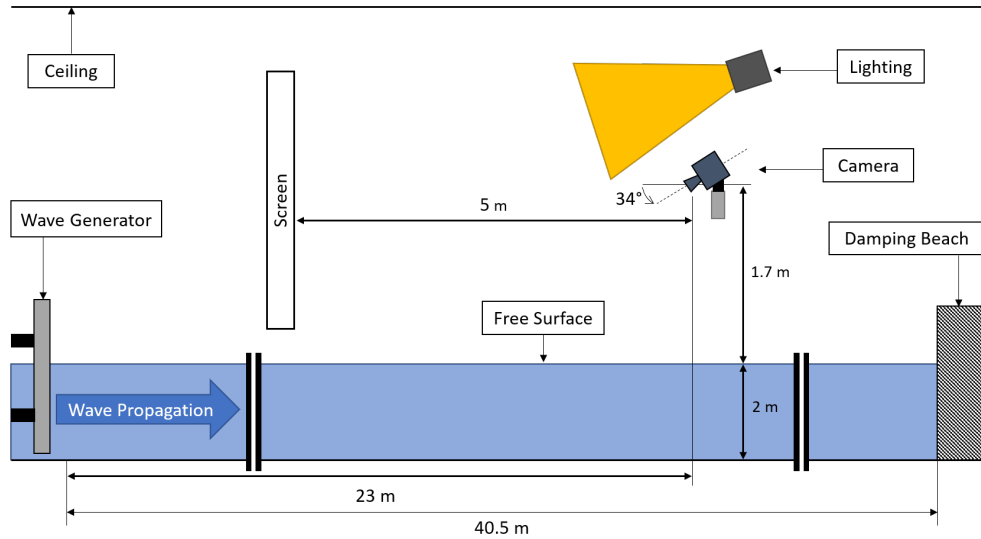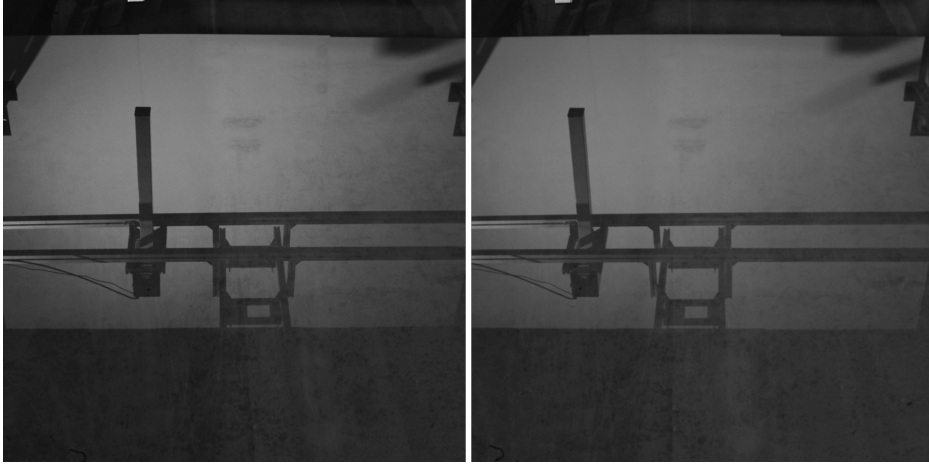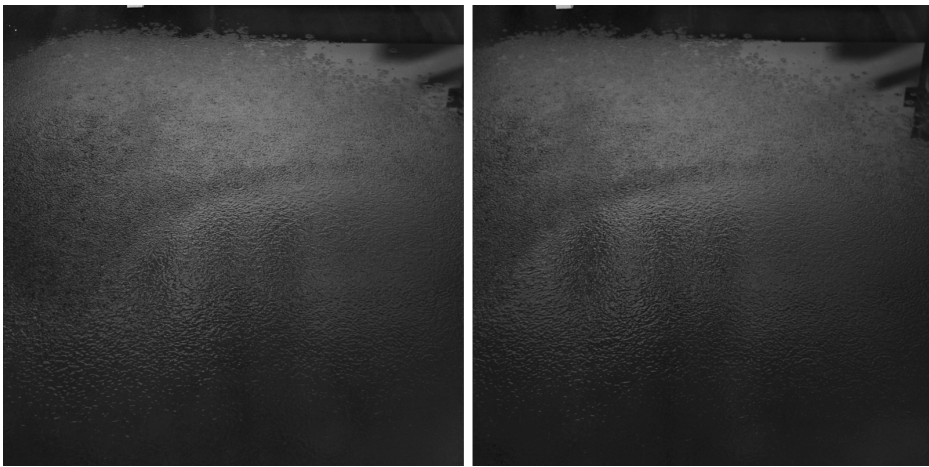
(a) Side view
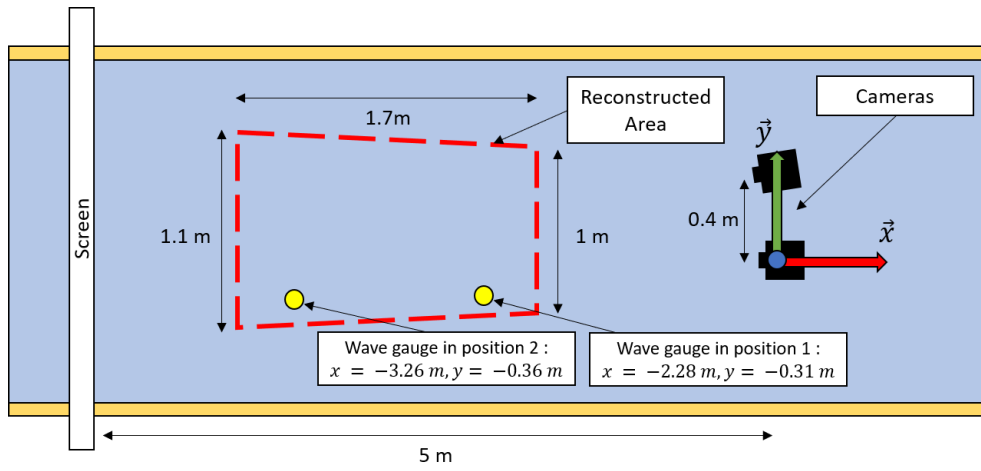
(b) Top view with wave gauge locations

Fig. 3: Diagrams of the experimental setup

totally blurred by the shortwaves in figure 4b, except for the top right corner which is not attained by the water droplets.

(a) Without short waves

(b) With short waves

Fig. 4: Impacts of the short-wave generation on the still free surface in the wave flume (left and right camera views)

2.3 Experimental Protocol

The main objective of this study is to compare measurements realized with a non intrusive servo-controlled wave gauge and the free-surface stereo-video reconstructions. To this end, four different regular waves conditions have been run several times in the flume. These conditions are described in table 1. In this table, as well as in the rest of the paper, H represents the wave height and T the wave period. The wave steepness ε is defined as $\varepsilon = k\frac{H}{2}$, k being the wave number. The relative depth kh is also given in this table, with h representing the wave-tank depth ($h = 2$ m).

Table 1: Regular wave conditions

Condition N°	H [m]	T [s]	ε	kh
1	0.06	1	0.12	8.05
2	0.1	1	0.20	8.05
3	0.2	2	0.10	2.08
4	0.3	1.5	0.27	3.58

For each case, the wave gauge measurements are performed in two different locations, further or closer to the cameras, in order to assess the accuracy of the stereo-video reconstructions at different distances from the cameras. The location of the different wave gauges is defined in figure 3b which depicts a top view of the experimental set-up. The wave gauge measurements and stereo-video measurements for the same wave conditions are performed during different runs, making use of the repeatability of the experiments, for two main reasons. The first is that the free surface beneath and behind the gauge is not well reconstructed when the tip of the wave gauge is out, because it is masking the scene behind. The second reason is that the gauge gets sprayed while watering the free-surface to create short waves, which makes the wave gauge vibrate and alters the quality of the wave-gauge measurements.

The stereo-video reconstruction process involves several steps. Firstly, given that the point cloud obtained after reconstruction is expressed in the left camera coordinates system, it is necessary to transport the points in the wave-flume coordinate system. The $x - y$ plane of the wave-flume reference frame is the still free surface and the origin is centered on the x and y coordinates of the left camera optical center. For this, the still free-surface is reconstructed and a best fit algorithm is used to determine the coordinates of the median plane passing through the theoretically planar point cloud representing the still free-surface. From the plane coordinates, it is possible to calculate the transformation from the left camera coordinates system to a flume coordinate system where the still free-surface would be a plane of coordinates $z = 0$ (mean free-surface level in the flume). The transformation is used afterwards to transport the different reconstructions in the flume reference frame. Once the transformation from the left camera frame to the flume reference frame is known, the free-surface reconstructions can be analyzed. Before analyzing the stereo-video reconstructions, the outliers are removed, *i.e.*, all the points whose z-coordinates are not included within the interval $z = \left[\frac{-H}{2} - 0.05; \frac{H}{2} + 0.05\right]$ m are removed. Once the outliers are removed, the point cloud is linearly interpolated on a regular mesh ($\Delta x = \Delta y = 10$ mm) and a z-coordinate median filter is applied over a 60 by 60 mm window. Figure 5 illustrates the different steps leading to the interpolated free-surface reconstruction of a regular wave (H=0.1 m, T=1 s).

Thanks to the interpolation, the free-surface elevation can be evaluated at any point of the mesh. Thus, the free-surface elevation at the location of the wave gauge can be extracted and compared to the reference wave-gauge measurements. To determine accurately the (x, y) location of the tip of the wave gauge in the flume coordinates, an image of the wave gauge with the tip of the wave gauge in contact with the water is recorded by both cameras while the water in the flume remains still. Subsequently,
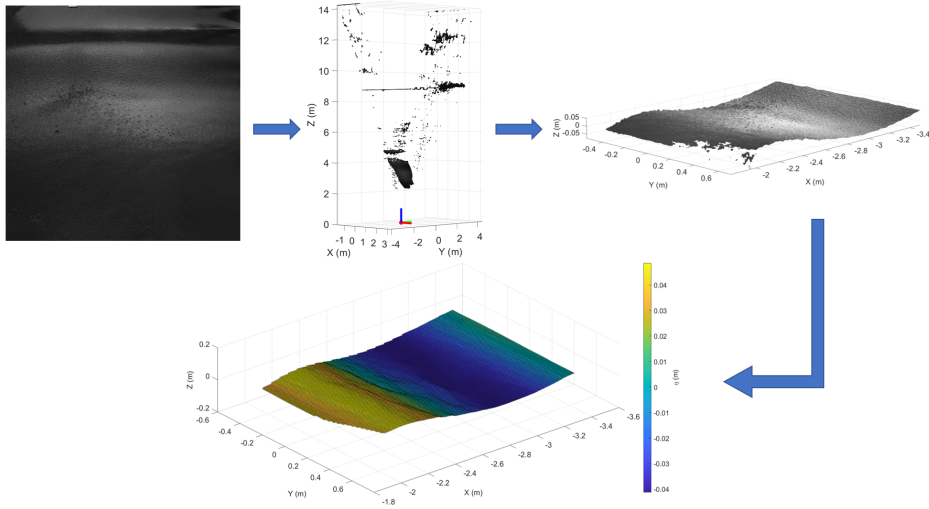
Fig. 5: Different steps of a free-surface reconstruction of regular waves (H=0.1 m, T=1 s). Up, from left to right : left camera view of the reconstructed area; reconstructed point cloud in the left camera coordinates frame; point cloud in the flume coordinates frame (outliers removed). Down : linear interpolation of the point cloud

the coordinates of the pixel representing the contact between the tip of the gauge and the free surface is manually located on both images of the stereo pair. From these coordinates and knowing the calibration parameters (intrinsic and extrinsic) of the stereo-rig, the tip location can be triangulated, expressed within the left camera frame and finally transported in the flume coordinates. Therefore, the interpolated free-surface elevation at the location of the tip of the wave gauge can be compared to the wave-gauge signal. Consequently, our comparisons between the wave gauge measurements and the stereo-video measurements rely on the repeatability of the regular waves generation in the wave flume. This has lead us to an assessment of both the wave-generator and the wave-gauge measurement repeatability, which is described in section 2.4.

2.4 Assessment of the wave-gauge and wave-generator repeatability

The repeatability of the water waves generated in the flume, and consequently of the wave-gauge measurements, is done as followed: each wave condition studied during the campaign is ran 3 to 4 times and measured with the wave gauge in one point. As the wave gauge recording is triggered by the wave generator, the different recordings with the same wave conditions can be compared to each other. As an indicator of the repeatability, the root-mean-square error (RMSE), defined as the square root of the mean quadratic difference between two signals, is calculated for each pair, over a duration of 20 seconds. Let us consider two wave-gauge recordings x_1 and

9

x_2 of measurements made at the same location with the same wave conditions. The recordings, of N=2500 samples each (20 s at 125 Hz), start once the periodic regime is established. The RMSE between these two signals is thus calculated by the following equation :

$$\text{RMSE} = \sqrt{\frac{1}{N} \sum_{n=1}^{N} (x_{1,n} - x_{2,n})^2} \qquad (1)$$

An average RMSE is calculated for each wave condition by averaging the RMSE computed for each pair over the different repeatability runs made with the same conditions. The normalized average relative error, $\frac{\text{RMSE}}{H}$, is obtained by dividing the average RMSE value by the wave height, H. The results obtained for the different wave conditions are summarized in Table 2.

Table 2: Estimation of the repeatability of the water-wave generation and the wave-gauge measurements

H [m]	T [s]	Average RMSE [mm]	Average relative error [%]	N° of runs
0.06	1	0.47	0.79	3
0.1	1	0.98	0.98	4
0.2	2	0.96	0.48	4
0.3	1.5	3.65	1.22	3

One can see that the waves with the smallest steepness (H=200 mm, T=2 s) are more repeatable than the waves with the highest steepness (H=100 mm, T=1 s & H=300 mm, T=1.5 s).

3 Analysis of the stereo-video measurements and results

In this section, we present different analyses of the free-surface stereo-video reconstructions obtained with the set-up described earlier in section 2. Section 3.1 is dedicated to the study of the accuracy of the still free-surface reconstructions. An assessment of the measurement accuracy for regular waves is presented in section 3.2. The free-surface profiles obtained with the stereo-video system are analyzed in section 3.3. Finally, a spectral analysis of the free-surface elevation is presented in section 3.4.

3.1 Still free-surface reconstruction

Let us analyze the free-surface reconstructions performed along the experimental campaign when the water was at rest. In such conditions, the free surface is assumed to be perfectly flat and therefore the accuracy of the reconstruction technique can be precisely assessed. The first analysis consists in evaluating the dispersion of the reconstructed points around the mean plane computed from the point cloud. This analysis

has been made for five different cases. For each case, 20 free-surface reconstructions were made to establish time averaged values.

Table 3: Static error on still free-surface reconstructions

Case n°	Date [dd/mm hh:mm]	Average MWL [mm]	Average σ_z [mm]
1	28/09 15:30	7.96	1.51
2	30/10 16:25	0.17	2.38
3	31/10 10:18	-0.02	2.26
4	31/10 16:45	0.03	2
5	03/11 10:13	-0.9	1.91

Table 3 summarizes the average values obtained for the five different cases in terms of mean water level (MWL) and root-mean-square values (or standard deviations), σ_z, of the distance between the reconstructed points and the MWL. For each case, the MWL is calculated relative to a reference level (MWL = 0 mm) established from the reconstruction of a single frame of case n°3 (chosen arbitrarily). Note that the variation of the MWL through time provides evidence of a decreasing water depth over time, as mentioned in section 3.2. The MWL decreased of almost 9 mm in 36 days. Among these five cases, the average value of σ_z goes from 1.51 mm to 2.38 mm around the MWL. Given that the camera and lighting set-ups have not changed between the different cases, and at the sight of the order of magnitude of these standard deviations, the short waves generated on the free surface probably have an important contribution to the measured standard deviation values. Hence, given that the light rain is watered manually, it cannot be always done in the same way, which in turn may induce variations in the scattering of the point cloud around the mean water level (or the standard deviation). The differences in terms of standard deviation observed between the different tests may also be explained by the presence of parasitic surrounding lights disturbing the reconstruction. However, the values of the standard deviations are very low and very close to each other, which demonstrates the good accuracy and repeatability of the proposed approach.

Let us now analyse more finely the accuracy of the free-surface reconstruction in the different regions of the reconstructed area. In contrast to section 3.1, the following analysis is based on interpolated and filtered data obtained from a 5 second measurement of the free-surface elevation. Figures 6a and 6b show the distribution of the time averaged local free-surface elevation, η_{mean}, and the local standard deviation (in time) of the free-surface elevation, σ_η, respectively. Note that the values depicted in these figures are restricted to the locations where there was no missing values over the measurement duration (5 seconds). One can see in figure 6a that the local mean free-surface elevation remains in the interval ± 2 mm except for a region close to point n° 2, which corresponds to the location of the wave gauge in position 2, where the mean free-surface elevation reaches a value of about 14 mm. The local standard deviation of the free-surface elevation depicted in figure 6b is below 2 mm over the majority of the reconstructed area. However, rather large values are observed in the bottom left

11

area. The time evolution of the local free-surface elevation at the different locations represented by colored crosses in figures 6a and 6b is depicted in figure 6c. As the free-surface remains still during the five seconds, the local time evolution of the free-surface elevation and its standard deviation provides an estimate of the measurement "noise" at the different locations. Apart from point n° 2, the maximum value of σ_η in the different location is 1.47 mm. For half of the regions, σ_η is lower than 1 mm, and equal to 1.08 mm for point n° 1, which is very small. The values of σ_η do not seem to be correlated with the location of the points. Note that point n° 6, which is located a bit further from the cameras, sees the value of σ_η increasing to 1.47 mm. In addition to the larger distance to the cameras, this higher value of σ_η may also be explained by a lower quality of the texture in this area. Indeed, it was rather difficult to create a uniform watering of the free surface over the entire reconstructed area. Hence, we had either to focus the watering on the closest or the furthest regions of the surface. This is even more striking for point n°2 whose standard deviation is equal to 14.85 mm. This case illustrates perfectly the limits of our texture generation method. The lack of short waves on the free-surface around point n°2 induces either a lack of reconstructed points ($t < 1.6$ s) or a very noisy signal that prevents from any reliable analysis. The short-wave generation system may be easily improved, for example using an omni-directional atomization device. Nevertheless, the accuracy of the measurements is very good despite the rather crude watering system used in our study and figure 6 shows that it is possible to obtain accurate results over a rather large area. In the experiments which were used to assess the accuracy of the approach for the measurement of water waves through comparisons with wave gauge measurements (following sections 3.2 to 3.4), the water gun was oriented in favour of the regions where the wave gauges were located.
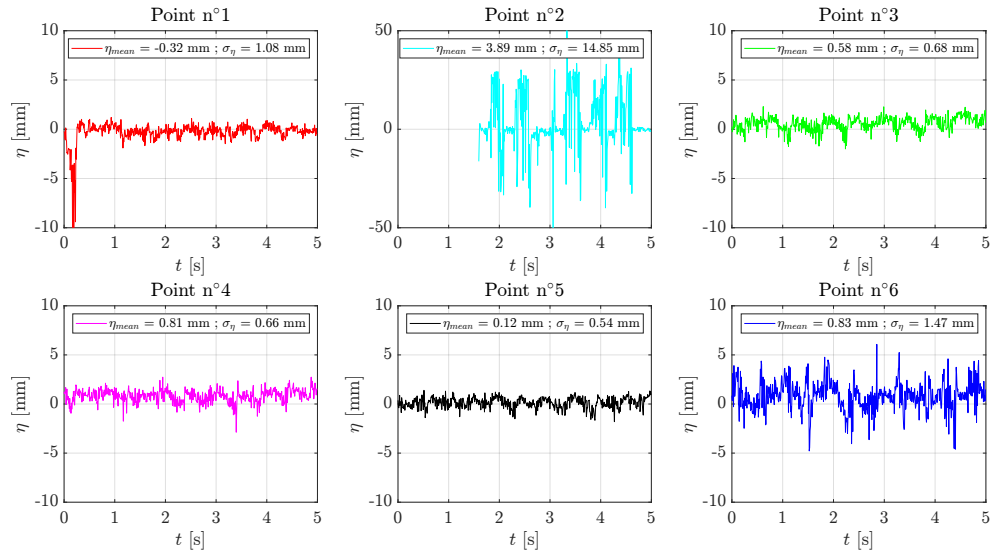
12
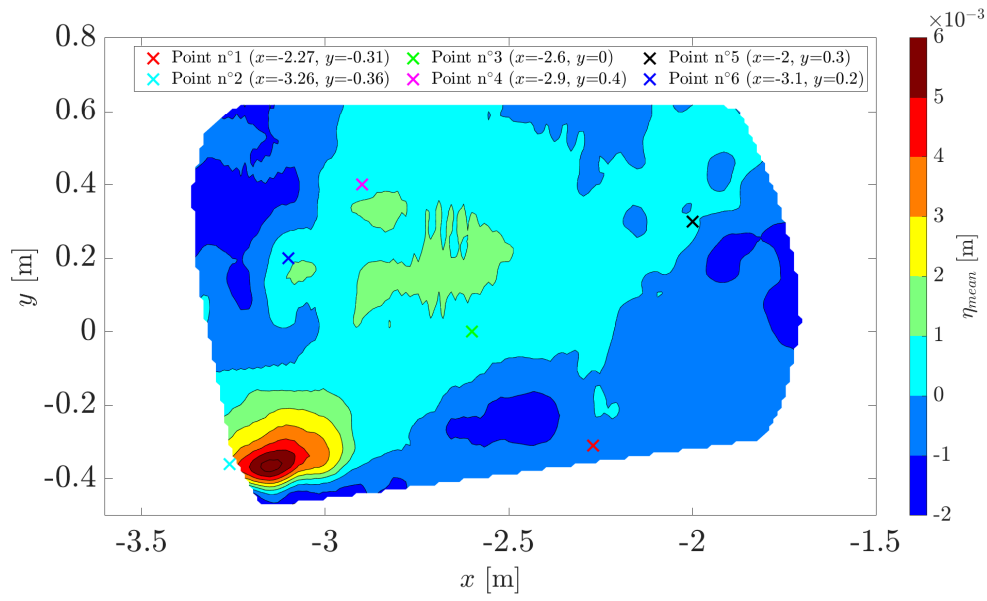
(a) Colormap of the local mean free-surface elevation η_{mean}
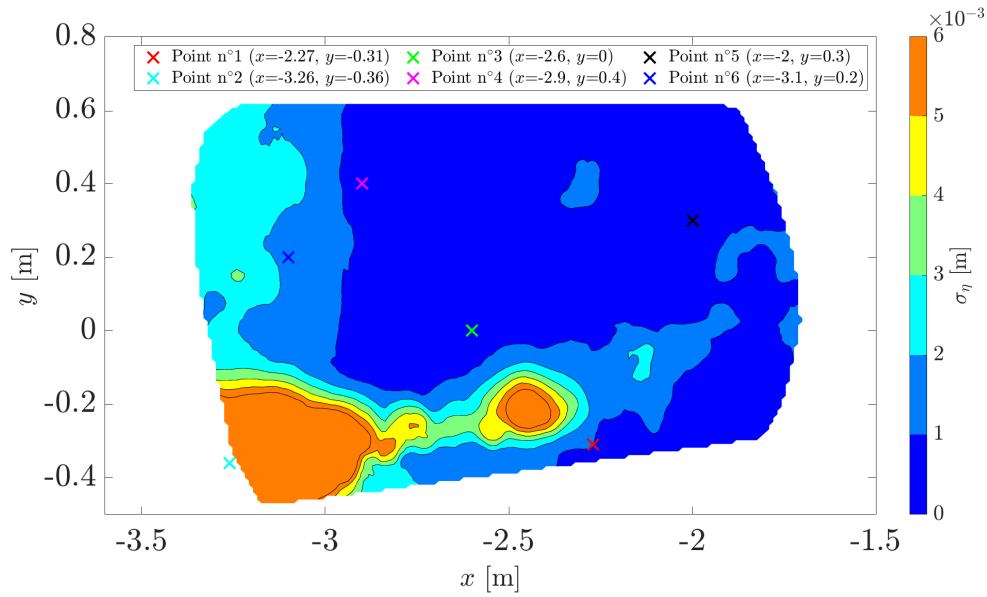
(b) Colormap of the standard deviation of the local free-surface elevation σ_η

Fig. 6: Evaluation of the measurement noise in different regions of a still free-surface reconstruction over 5 s

13

(c) Free-surface elevation at each location over 5 seconds

Fig. 6: Evaluation of the measurement noise in different regions of a still free-surface reconstruction over 5 s

14

3.2 Comparison between the wave-gauge measurements and the stereo-video measurements

As mentioned in section 2.3, the free-surface elevation was measured at two locations with a servo-controlled wave gauge. Note that only a single comparison is made, for each wave condition, between the stereo-video and the wave-gauge measurements when studying the position 1 (x=-2.28 m, y =-0.31 m in the flume coordinate system).

It is important to emphasize that sometimes the tip of the wave gauge would start vibrating due to electromagnetic interferences, hence generating noisy measurements. On the other hand, as mentioned in section 3.1, the texture created by watering the free-surface is not always homogeneous and perfect, leading to non reconstructed zones or small outliers. As noisy wave gauge signals or bad reconstructions would alter our comparisons, we selected signal samples during which both signals were of sufficiently good quality. Hence both methods are compared over a duration of two to three wave periods.

Table 4: Results of RMSE Analysis between wave gauge measurements and stereo video measurements

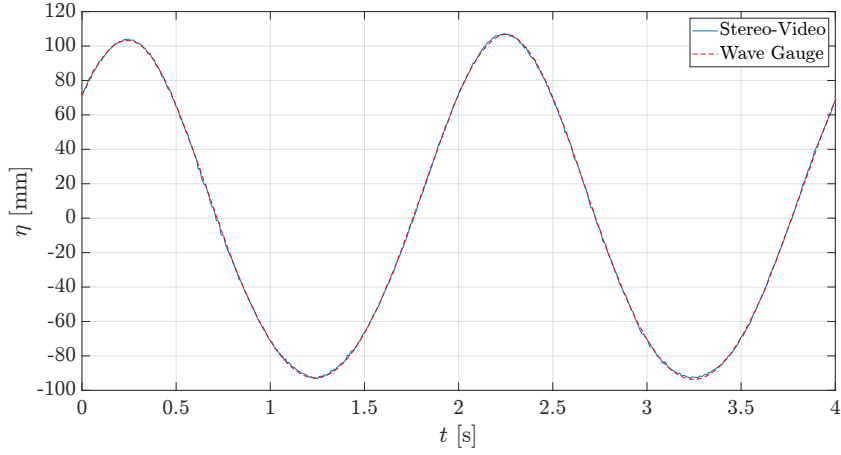|		Wave gauge in position 1		Wave gauge in position 2	
H [m]	T [s]	RMSE [mm]	Relative error [%]	RMSE [mm]	Relative error [%]
0.06	1	0,87	1.45	1.83[1]	3.04[1]
0.1	1	1.62	1.62	2.71[2]	2.71[2]
0.2	2	0.81	0.41	5.14	2.57
0.3	1.5	2.23	0.74	/	/

[1]Averaged over two stereo-video reconstructions

[2]Averaged over three stereo-video reconstructions

Table 4 shows the results for the two wave-gauge locations. For this analysis, we applied the same comparison method as the one used to assess the wave-gauge repeatability in section 2.4. Indeed, the root mean square difference between the wave-gauge measurements and the stereo-video measurements, *i.e.* the RMSE, is calculated for recordings made with the same wave conditions. The relative error, in percentage, is then calculated as : Relative error $= \frac{\text{RMSE}}{H}$.

As one can see, there are no results for the conditions ($H = 0.3$ m, $T = 1.5$ s) for position 2 (where the gauge is the furthest from the cameras). Indeed, due to the wave steepness and the grazing angle of the cameras, the troughs of the waves are not well reconstructed, resulting in incomplete stereo-video data at position 2 (this will be discussed further in section 3.5).

The most obvious observation to make from this table is the fact that the reconstruction seems more accurate (or at least closer to the wave gauge measurements) for measurements made closer to the cameras. This is principally related to the fact that the resolution of the reconstruction is finer close to the cameras. To give an order of magnitude, at 3.26 m from the cameras (gauge in position 2), a pixel represents approximately 1.87mm, while a pixel represents approximately 1.29 mm at 2.28m from

(a) Wave gauge in position 1
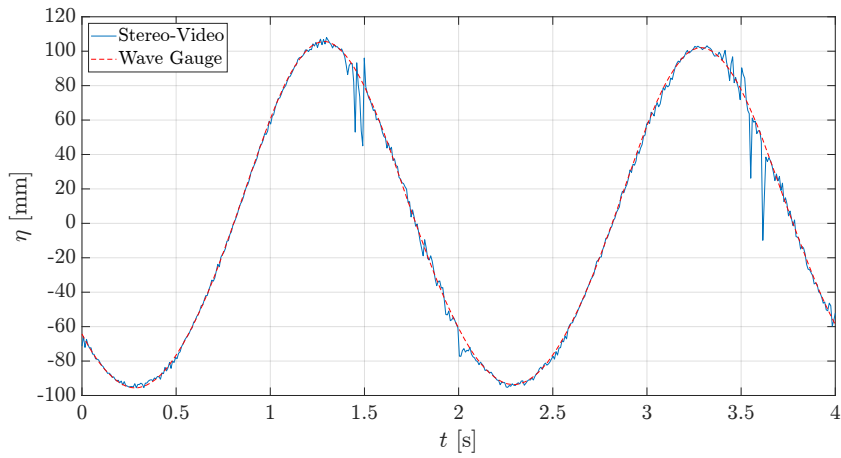
(b) Wave gauge in position 2

Fig. 7: Comparison between measurements made with the servo-controlled wave gauge and the virtual wave gauge from stereo-video reconstructions in pos.1 and pos.2 - Wave conditions : $H = 0.2$ m, $T = 2$ s

the cameras (position 1). Therefore, the closer the free-surface is from the camera, the more accurate the measurements should be. Another observation to be made is that the stereo-video measurements are the closest to the wave-gauge measurements for the waves displaying the best repeatability (see section 2.4). It is also important to note that the RMSE values are of the order of magnitude of the wave-gauge accuracy.

Figure 7 shows comparisons of the free-surface elevation measurements made with the stereo-video system and with the servo-controlled wave gauge at position 1 and position 2. In figure 7a, both signals almost overlap, which is in accordance with the very low error reported for position 1 in table 4. For position 2 (see figure 7b),

the error increase is explained by the discrepancies just after the crest of the waves has passed under the gauge. The stereo-video measurements obtained for ($H = 0.1$ m, $T = 1$ s) depicted in figure 8 do not present such sharp irregularities, but some small perturbations are visible in the back of the waves on the stereo-video signal corresponding to position 2. It will be shown in the following sections that the front of the waves are more accurately reconstructed than the back of the waves, especially for the largest steepness waves.

Nevertheless, despite the small discrepancies, the noisy measurements and the decrease in accuracy through distance, the results are very encouraging and show the ability of the stereo-video free-surface reconstruction technique to perform measurements with an accuracy relatively close to a servo-controlled wave-gauge (maximum 3.04% of error about 3.3m from the cameras) over a surface of 1.1m by 1.7m.

Note: During the experiments, we noticed lately (after performing the measurements with the wave gauge in position 1) a decrease in the mean water level. Consequently, several days separate the last measurements from the water level reference made with the stereo-video system, hence generating an offset between the wave-gauge signals and the virtual-gauge signals. To overcome this issue (only for the measurements made with the wave gauge in position 1), the mean value of both signals have been subtracted to make the comparisons possible (only for the free-surface elevation at position 1).
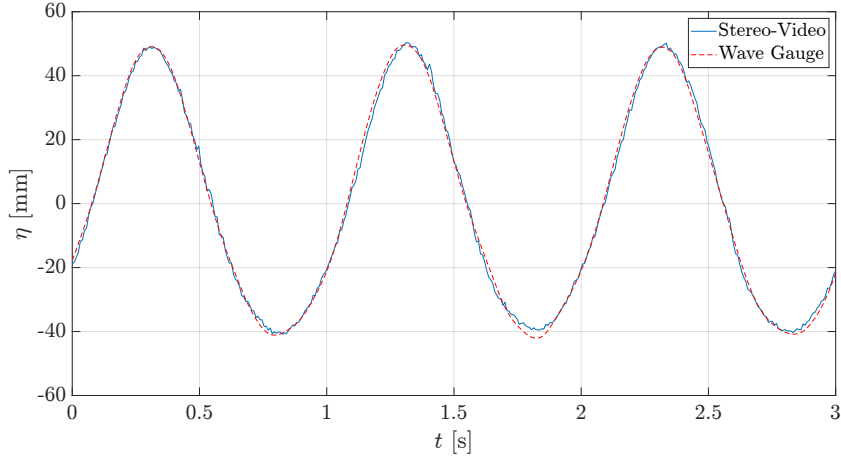
(a) Wave gauge in position 1
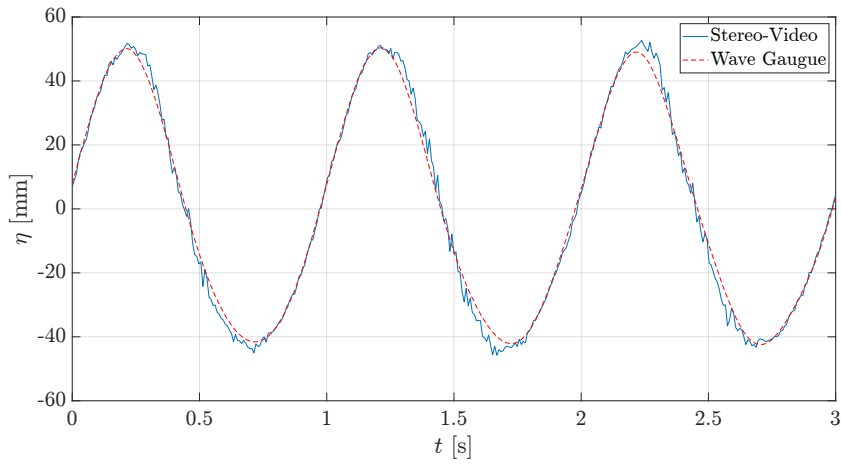
(b) Wave gauge in position 2

Fig. 8: Comparison between measurements made with the servo-controlled wave gauge and the virtual wave gauge from stereo-video reconstructions in pos.1 and pos.2 - Wave conditions : $H = 0.1$ m, $T = 1$ s

3.3 Free-surface profile analysis

One of the interests of the stereo-video approach is the ability to measure the free-surface elevation at different locations at the same instant. In a free-surface reconstruction interpolation, the location and quantity of the measured points is controlled by the mesh definition. Figure 9 depicts an interpolation in which the free-surface elevation can be evaluated in 25375 different locations. Measuring the elevation in a regular grid allows to observe free-surface profiles along a specific axis. For instance, the red curve shown in figure 9 represents the free-surface profile along $y = 0$.
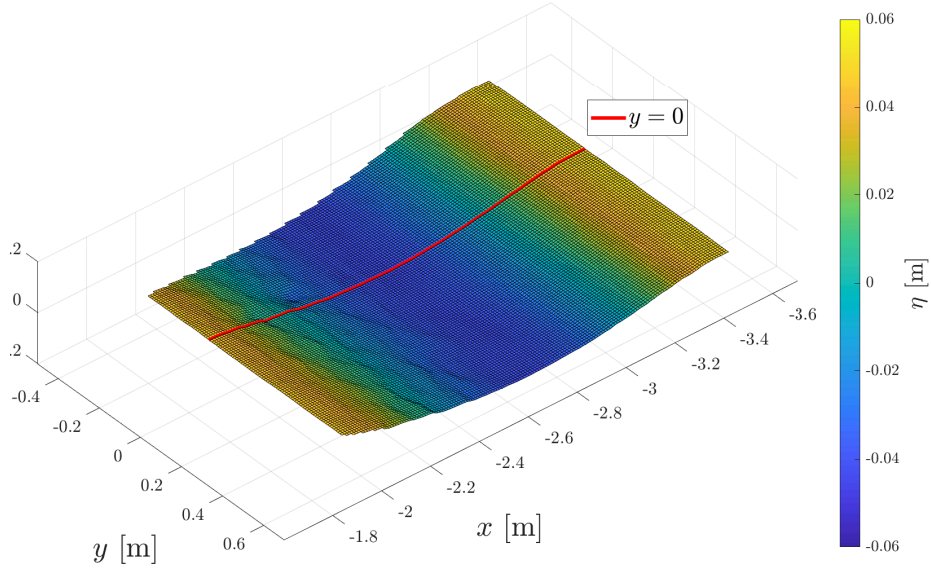
Fig. 9: Interpolated free-surface reconstruction at $t = t_0 + 0.7T$ ($H = 0.1$ m, $T = 1$ s)

This means that the stereo-video approach makes it possible to analyze the time-evolution of the free-surface profile along a specific direction. For the sake of illustration, eleven free-surface profiles along $y = 0$ have been extracted from interpolations of the reconstructions of ($H = 0.1$ m, $T = 1$ s) over a single wave period (T). The results are depicted in figure 10. Note that the waves propagate along the x-axis towards the positive direction. As the period of the waves is $T = 1$ s, each profile depicted in figure 10 shows almost an entire wave-length ($\lambda \approx 1.56$ m). In this figure, the red curve showing the free-surface profile at $t = t_0 + 0.7T$ in figure 9 is represented by the blue-sky curve. The profiles presented in figure 10 show some perturbations (the profiles are a little bit wavy and not perfectly smooth). These perturbations seem to affect more the back of the waves than the front of the waves. Nevertheless, the amplitude of the perturbations is very small. Moreover, the profiles show a great consistency of the measurement through time and space.
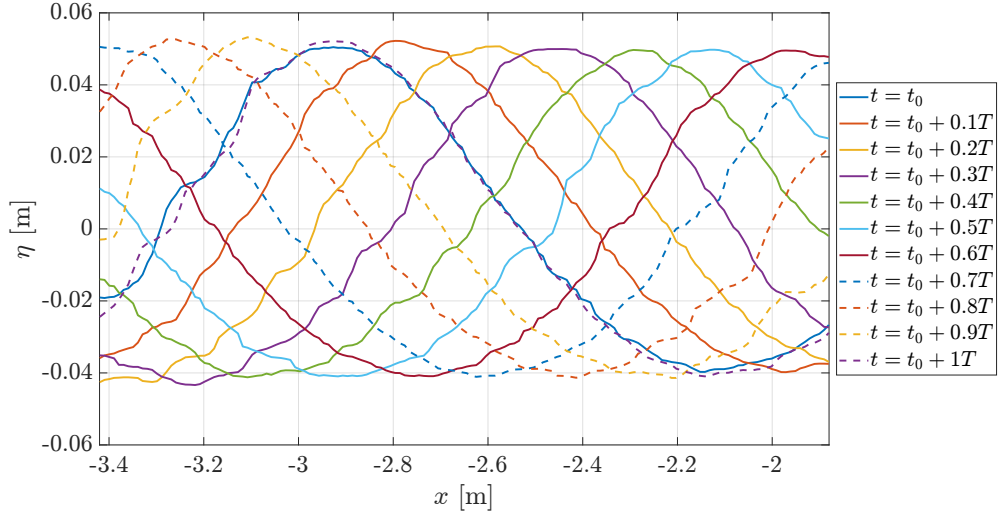
Fig. 10: Free-surface profiles along $y = 0$ m extracted from stereo-video reconstruction interpolations for $H = 0.1$ m, $T = 1$ s

3.4 Spectral analysis of wave case 2 (H=0.1m, T=1s)

In this section we analyse the frequency content of a time-series of stereo-video reconstructions of wave case 2 (H=0.1m, T=1s) in order to assess a possible effect of the short waves generated by the droplet impacts on the surface gravity waves generated by the wave paddle and to assess whether the stereo-video approach is suitable for a fine spectral analysis of the wave field. For this purpose, we have computed the amplitude spectra from a 10 s sample of the free-surface elevation for each point of the interpolated stereo-video reconstruction over the region corresponding to -3.17 m< x <-1.94 m and -0.26 m< y <0.45 m. The average spectrum obtained from these different spectra is depicted in figure 11 together with the amplitude spectrum computed from a wave gauge measurement of the same wave train. One can see that the energy distribution around the first three wave harmonics obtained from the two approaches are very close to each other. Indeed, the difference between the peak value of the first wave harmonic obtained with the two approaches is about 2%. However, the energy contained in the stereo-video amplitude spectrum above 4 Hz is larger than that of the wave gauge signal. This difference probably comes from the presence of high frequency capillary waves in the stereo-video measurements and the absence of this type of waves in the wave gauge measurements. The same high frequency content is visible in the average amplitude spectrum obtained from a 5 s stereo-video reconstruction series without surface gravity waves (calm water) also depicted in figure 11. Note however that the spatial resolution of the stereo-video reconstruction is insufficient to resolve the highest wave frequency components and that the stereo-video reconstruction approach may also induce additional high frequency noise. Based on these results, which were obtained with a rather short wave period (for this type facility), we can conclude that the short waves generated by the droplet impacts and the stereo-video
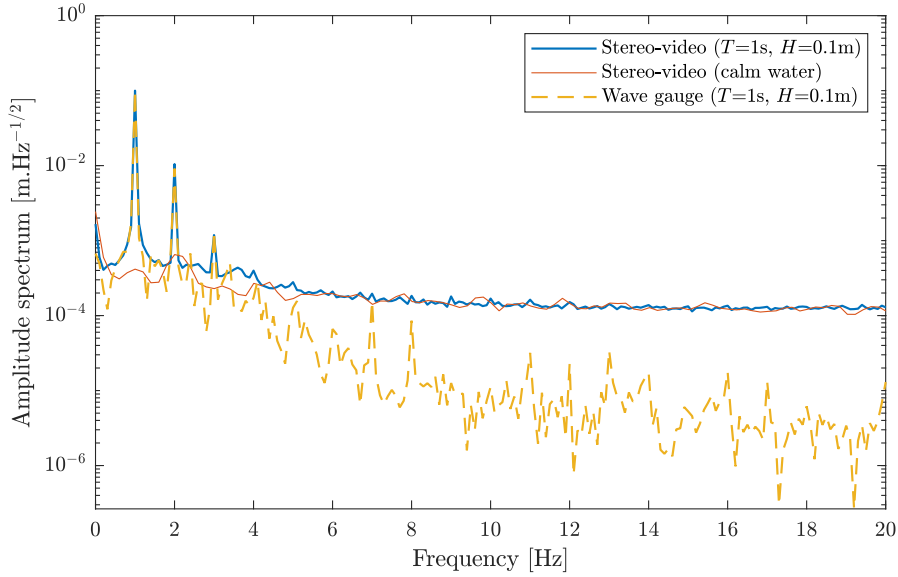
Fig. 11: Comparison of the free-surface elevation amplitude spectra obtained from the stereo-video approach and the wave gauge for wave case 2 (H=0.1m, T=1s). The amplitude spectrum obtained from a stereo-video reconstruction of the free-free surface without waves (calm water) is also shown for comparison.

reconstruction methodology do not affect the spectral content of the surface gravity waves.

3.5 Limitations of the approach

In this section, we discuss some limitations of the stereo-video approach. For example, we have mentioned in section 3.2 that the stereo-video measurements at the point corresponding to the wave gauge in position 2 were incomplete. This wave condition corresponds to the steepest ($\varepsilon = 0.27$) waves investigated in the current study (see table 1). With these conditions, the relative angle between the optical axis of the cameras and the free surface evolves in time and becomes too small for a good reconstruction when the back of the wave is in the field of view of the cameras. Indeed, it has been shown by Adam [11] that, when this relative angle gets lower than 20°, holes start to appear in the reconstructed surface, making it non exploitable for measurements. Hence, when the slope of the wave is too high, there is a risk that the back of the wave might not be reconstructed. On the contrary, the fronts and the crests of the waves are always well reconstructed as long as they are in the measurement field of the cameras. The small perturbations which appear in the back of the waves in figure 10 are likely to be a precursor of this problem, which appears to increase with the wave steepness, up to the point where the free-surface is no more reconstructed.

21

It appears that ($H = 0.3$ m, $T = 1.5$ s) is the only studied condition where the minimum relative angle between the free surface and the optical axis of the cameras is lower than 20°. The free-surface profiles along $y = -0.31$ m depicted in figure 12 illustrate this phenomenon. One can see that the fronts and the crests are reconstructed no matter their location within the measurement field. However, for the profiles at $t = t_0 + 0.1T$, $t = t_0 + 0.2T$ and $t = t_0 + 0.3T$, one can see that the back of the wave is missing. The three-dimensional point cloud of the reconstruction corresponding to $t = t_0 + 0.3T$ is depicted in figure 13. In this reconstruction, there there are many points in the crest of the wave, but there are very few reconstructed points in the back of the wave and no reliable measurement can be performed in this region. It is only from $t = t_0 + 0.5T$ that the back and the trough of the wave start being reconstructed. In figure 14, which depicts the three-dimensional point cloud of the reconstruction corresponding to $t = t_0 + 0.6T$, it can be observed that the region closest to the cameras, which corresponds to the back of the wave, is not well reconstructed because the slope starts to be important in this region. For $t \geq t_0 + 0.7T$, the free-surface profiles shown in figure 12 are complete, as only the through and the front of the wave are present in the measurement field. For the sake of illustration, the three-dimensional point cloud of the reconstruction corresponding $t = t_0 + 0.8T$ is depicted in figure 15. One can see that the front of the wave is perfectly reconstructed. The lack of free-surface profile at $x = -3.26$ m during almost half a period prevents us from comparing the wave-gauge measurements and the stereo-video measurements in position 2 with the present set-up. As the wave gauge is much closer to the cameras in position 1 ($x = -2.27$ m), there are very few instants where the relative angle between the optical axis and the free surface approaches 20°, hence the measurements are still possible.

Two solutions could be considered to overcome these limitations . The first solution could be to set the cameras higher and increase the initial grazing angle to prevent the relative angle between the free surface and the optical axis of the cameras from approaching 20°. Nevertheless, increasing the grazing angle increases the chance of seeing through the free surface (and seeing the bottom of the tank). The other solution would be to set the cameras perpendicular to the wave propagation direction. In this manner, the relative angle between the cameras and the free surface would not change significantly with the height and steepness of the waves.
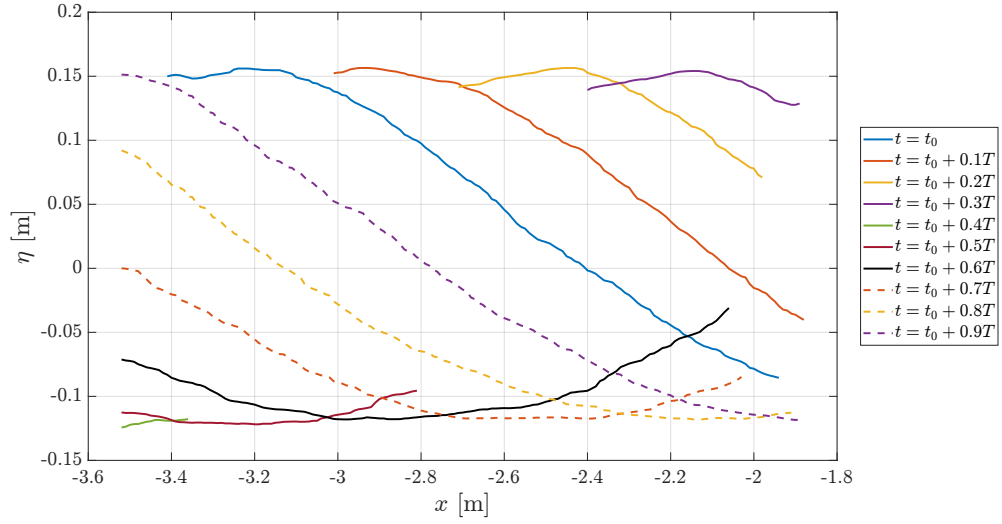
Fig. 12: Free-surface profiles along $y = -0.31$ m, extracted from stereo-video reconstruction interpolations for $H = 0.3$ m, $T = 1.5$ s
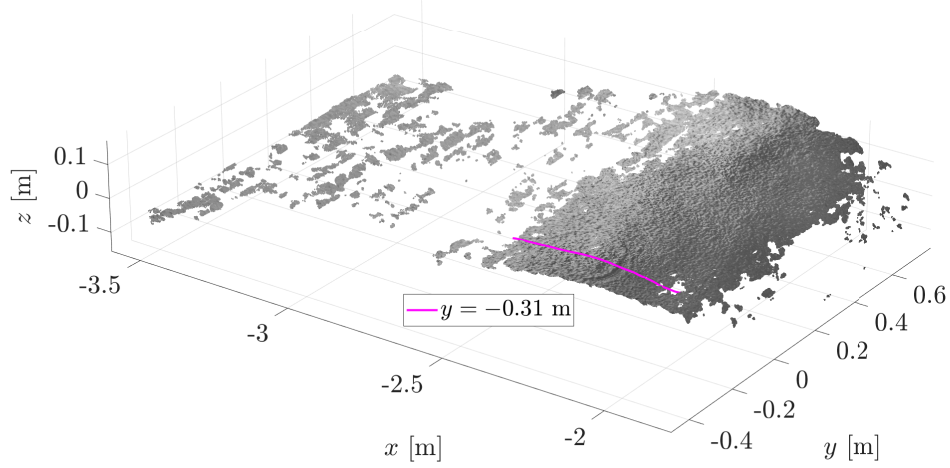

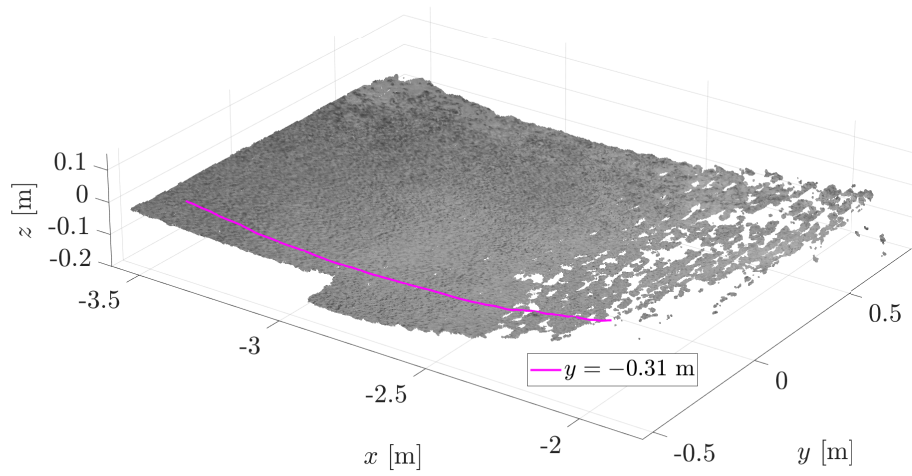**Fig. 13**: $H = 0.3$ m, $T = 1.5$ s - Free-surface reconstruction at $t = t_0 + 0.3T$

Fig. 14: $H = 0.3$ m, $T = 1.5$ s - Free-surface reconstruction at $t = t_0 + 0.6T$
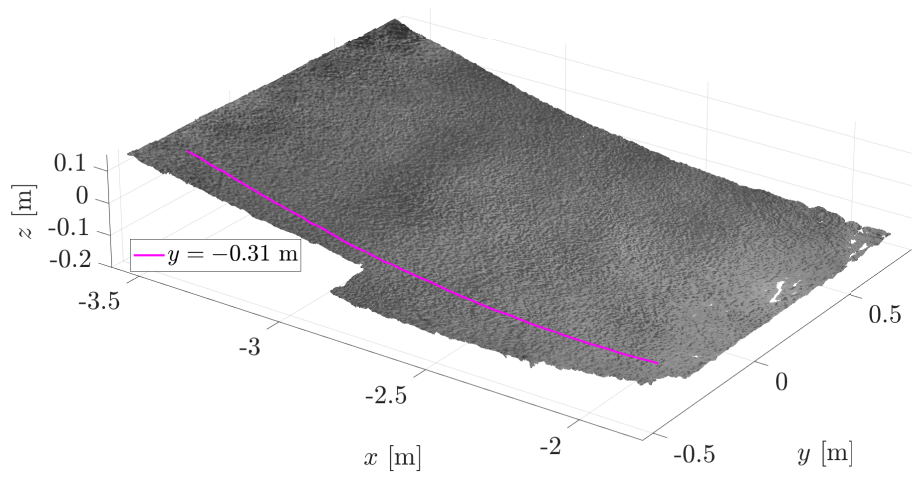

Fig. 15: $H = 0.3$ m, $T = 1.5$ s - Free-surface reconstruction at $t = t_0 + 0.8T$

4 Conclusion and prospects

We have presented a new stereo-video approach to perform high-resolution free-surface reconstructions in wave tank experiments. Unlike previous works, this technique does not require particle seeding but is based on a diffuse and homogeneous lighting device associated with a short wave generation system to increase the roughness of the free-surface. This approach was validated through the reconstructions of a still free surface and regular waves in a wave flume.

For the experimental implementation of this approach, two cameras were placed above the free-surface, facing the wave propagation direction. The diffuse lighting was generated by means of a wide white screen placed 5 m in front of the cameras and illuminated by LED lighting heads. The short waves, necessary to create some free-surface roughness, were generated by light rain droplet impacts on the free surface. The light rain was manually distributed by means of a watering gun. With this set-up, measurements can be performed on a trapezoidal area with a surface of 1.8 m^2.

The root mean square distance between the cloud points and the reconstructed still water mean plane varied from 1.51 mm to 2.38 mm depending on the reconstructions, which demonstrates the spatial accuracy of the system. In addition, a temporal study of the free-surface elevation at specific locations of the still free surface allowed us to show the consistency of the measurements through time. This study also showed that further developments have to be done to make the short-wave generation spatially more homogeneous and stationary, and to extend the impacted area.

The accuracy of the stereo-video measurement system for the reconstruction of the free-surface during regular wave experiments was assessed through comparisons with wave-gauge measurements in different regions of the reconstructed surface. Beforehand, the accuracy and repeatability of the wave-gauge measurements was evaluated to a maximum error of 1.2%. In comparison with the wave-gauge measurements, the maximum relative error observed with the stereo-video system was about 2.5%. Even if the measurement error is a little more important than with the wave gauge, the possibilities offered by the free-surface elevation field measurements and the gains in terms of set-up flexibility for experimental studies are considerable. As an order of magnitude, the free-surface reconstruction presented in figure 15 contains about 700 000 reconstructed points. These results are all the better for the fact that the measured points were located at the left edge of the reconstructed zone, more subject to noisy signals and reconstruction discrepancies. Better result are also to be expected with an improved short-wave generation device.

A discrete Fourier transform of the free-surface elevation time series obtained from the stereo-video approach was performed in order to assess the effect of the water droplet impacts on the surface gravity waves generated by the wave paddle. The amplitude spectra of the free-surface elevation obtained from the stereo-video approach are very close to those obtained from the Fourier transforms of the wave-gauge signal. These comparisons, which were performed with a rather short wave train ($T = 1$ s, $H = 0.1$ m), show that the texture and the stereo-video approach do not alter the spectral content of the surface gravity waves. This conclusion is particularly promising for future investigations on irregular waves.

Finally, free-surface profiles along the y-axis were realized and showed a great consistency of the measurement through time and space. The analysis also pinpointed that particular attention has to be given not to set the cameras in a way that the angle between the optical axis and the free surface gets lower than 20°.

We are planning to use this method for the measurement of the wake of a ship model in a towing tank. Further work will also aim at adapting the technique to the measurement of breaking waves (up to the breaking inception).

Declarations

Competing interests. The authors have no competing interests to declare that are relevant to the content of this article.

Availability of data and materials. Raw and derived data supporting the findings of this study are available from the corresponding authors upon reasonable request

Authors' contributions. S.LP., A.T. and J.C. conceptualized the methodology. S.LP., A.T. and J.C. developed the experimental set-up and performed the experiments. S.LP. and A.T. analyzed the results and wrote the main manuscript text. A.T. and G.D. wrote the grant application and coordinated the project. All authors reviewed the manuscript.

References

[1] Chabchoub, A., Mozumi, K., Hoffmann, N., Babanin, A.V., Toffoli, A., Steer, J.N., Bremer, T.S., Akhmediev, N., Onorato, M., Waseda, T.: Directional soliton and breather beams. Proceedings of the National Academy of Sciences **116**(20), 9759–9763 (2019)

[2] McAllister, M.L., Draycott, S., Adcock, T., Taylor, P., Van Den Bremer, T.: Laboratory recreation of the draupner wave and the role of breaking in crossing seas. Journal of Fluid Mechanics **860**, 767–786 (2019)

[3] Swan, C., Sheikh, R.: The interaction between steep waves and a surface-piercing column. Philosophical Transactions of the Royal Society A: Mathematical, Physical and Engineering Sciences **373**(2033), 20140114 (2015)

[4] Gomit, G., Chatellier, L., David, L.: Free-surface flow measurements by non-intrusive methods: a survey. Experiments in Fluids **63**(6), 94 (2022)

[5] Moisy, F., Rabaud, M., Salsac, K.: A synthetic schlieren method for the measurement of the topography of a liquid interface. Experiments in Fluids **46**(6), 1021–1036 (2009)

[6] Gomit, G., Chatellier, L., Calluaud, D., David, L.: Free surface measurement by stereo-refraction. Experiments in Fluids **54**(6), 1540 (2013) https://doi.org/10.1007/s00348-013-1540-4 . Accessed 2023-04-24

[7] Aubourg, Q., Campagne, A., Peureux, C., Ardhuin, F., Sommeria, J., Viboud, S., Mordant, N.: Three-wave and four-wave interactions in gravity wave turbulence. Physical Review Fluids **2**(11), 114802 (2017)

[8] Savelyev, I., Fuchs, J.: Stereo thermal marking velocimetry. Frontiers in Mechanical Engineering **4**, 1 (2018)

[9] Przadka, A., Cabane, B., Pagneux, V., Maurel, A., Petitjeans, P.: Fourier transform profilometry for water waves: how to achieve clean water attenuation with diffusive reflection at the water surface? Experiments in fluids **52**, 519–527 (2012)

[10] Aubourg, Q.: Étude expérimentale de la turbulence d'ondes à la surface d'un fluide. la théorie de la turbulence faible à l'épreuve de la réalité pour les ondes de capillarité et gravité. PhD thesis, Université Grenoble Alpes (ComUE) (2016)

[11] Adam, T.: Mesures Stéréo-vidéos en bassin d'essais **Rapport de fin d'études** (2021)

[12] Caplier, C., Rousseaux, G., Calluaud, D., David, L.: Energy distribution in shallow water ship wakes from a spectral analysis of the wave field. Physics of Fluids **28**(10) (2016)

[13] Benetazzo, A.: Measurements of short water waves using stereo matched image sequences. Coastal Engineering **53**(12), 1013–1032 (2006) https://doi.org/10.1016/j.coastaleng.2006.06.012 . Accessed 2023-02-22

[14] Bergamasco, F., Torsello, A., Sclavo, M., Barbariol, F., Benetazzo, A.: WASS: An open-source pipeline for 3D stereo reconstruction of ocean waves. Computers & Geosciences **107**, 28–36 (2017) https://doi.org/10.1016/j.cageo.2017.07.001 . Accessed 2023-04-24

[15] Leckler, F.: Observation and modelisation of wave breaking. PhD thesis, Brest (2013)

[16] Le Page, S., Tassin, A., Caverne, J., Gall, Y.L., Gomez, B., Ducrozet, G.: Towards accurate stereo-video based free-surface reconstruction for wave tank experiments. IOP Conference Series: Materials Science and Engineering **1288**(1), 012009 (2023) https://doi.org/10.1088/1757-899X/1288/1/012009 . Publisher: IOP Publishing. Accessed 2024-01-23

[17] MATLAB: Estimate geometric parameters of a stereo camera - MAT-LAB - MathWorks France (2023). https://fr.mathworks.com/help/vision/ref/stereocameracalibrator-app.html Accessed 2023-04-19

[18] Bouguet, J.-Y.: Camera Calibration Toolbox for Matlab. (2008). http://robots.stanford.edu/cs223b04/JeanYvesCalib/ Accessed 2023-02-22

[19] Zhang, Z.: A flexible new technique for camera calibration. IEEE Transactions on Pattern Analysis and Machine Intelligence **22**(11), 1330–1334 (2000) https://doi.org/10.1109/34.888718 . Conference Name: IEEE Transactions on Pattern Analysis and Machine Intelligence

[20] Heikkila, J., Silven, O.: A four-step camera calibration procedure with implicit image correction. In: Proceedings of IEEE Computer Society Conference on Computer Vision and Pattern Recognition, pp. 1106–1112 (1997). https://doi.org/10.1109/CVPR.1997.609468 . ISSN: 1063-6919